Gondwana Research 116 (2023) 12–24

Contents lists available at ScienceDirect

Gondwana Research

journal homepage: www.elsevier.com/locate/gr

GR Letter

Supercontinent-paced magmatic destabilisation and recratonisation of the Yilgarn Craton

A.R.A. Aitken [a,*], M. Fiorentini [a], M. Tesauro [b,c], N. Thébaud [a]

[a] Centre for Exploration Targeting, School of Earth Sciences, The University of Western Australia, Perth, Western Australia, Australia
[b] Dipartimento di Matematica e Geoscienze, Università di Trieste, Trieste, Italy
[c] Utrecht University, Utrecht, Netherlands

ARTICLE INFO

Article history:
Received 4 July 2022
Revised 20 November 2022
Accepted 23 November 2022
Available online 4 January 2023
Handling Editor: M. Santosh

Keywords:
Craton
Lithosphere
Refertilisation
Supercontinent
Australia

ABSTRACT

Knowledge of the evolution of ancient cratonic lithospheres underpins our understanding of Precambrian Earth. The Yilgarn Craton has exceptionally well-preserved Archean geology, with juvenile crust formation and major orogenesis concluding in the Neoarchean, and a stabilised upper-crustal architecture developing before 2.42 Ga. However, in an apparent dichotomy, geophysical models resolve lithospheric mantle composition outside the range of xenolith data from Archean regions, indicating the lithospheric mantle has since been extensively refertilised. Post-Archean igneous and sedimentary rocks record a prolonged lithospheric evolution that is not well resolved in datasets recording bulk crustal isotopic evolution. Reconciling these, we combine interpretation of geological and geophysical data to resolve two phases of lithosphere destabilisation driven by major magmatic events at ~2.06 Ga and at ~1.08 Ga. During destabilisation, sub-lithospheric and sub-crustal mantle fluxes caused extensive mantle refertilisation. For 200–400 Ma post-refertilisation, distributed sedimentary basins formed during recratonisation of the now denser lithosphere. The timing of these events suggests a relationship with the early stages of supercontinent assembly: Dominant downwelling beneath the assembling supercontinent sustains a sufficiently non-tensile tectonic setting to inhibit lithospheric thinning and breakup and enhances lateral flow of any upwelling mantle. This setting allows widespread intraplate refertilisation to occur while later the assembled supercontinent provides a stable setting allowing thermal re-equilibration and recratonisation to occur. In contrast, lithospheric refertilisation during supercontinent breakup will be more susceptible to density instabilities and recycling in later collisions. Consequently, we suggest that refertilisation of extant cratonic lithosphere may dominantly have occurred during the assembly of supercontinents.

1. Introduction

The development of cratonic lithosphere has played a crucial role in the evolution of Precambrian Earth, and has an ongoing impact on our planet, including its mineral resources (Hoggard et al., 2020) and natural hazards (Huang et al., 2002). While the accessible crust may be studied in detail, a complete knowledge of lithosphere evolution also demands that processes in the mantle and deep crust are well understood.

Where targeted studies have been performed, the composition of the lithospheric mantle shows substantial diversity relating to the varied and often prolonged evolutions of continents (Afonso et al., 2021; Finger et al., 2022; Tang et al., 2013; Tesauro et al., 2020). Importantly, several key processes of the lithospheric mantle may be partially decoupled from that of the crust (Menzies et al., 2007; Wang et al., 2018; Zheng et al., 2012) and therefore the mantle may develop at different times to the crust. Consequently, we cannot assume that a detailed knowledge of the crust is sufficient to define a craton's evolution, and different approaches are needed to understand independently the mantle evolution.

This work focuses on the development of the lithospheric mantle of the Yilgarn Craton in Western Australia. We uncover a fundamental dichotomy between the formation of the crust in the Archean and the anomalously fertile composition of the lithospheric mantle, which for much of the craton extent is outside the global range for xenolith data from Archean cratons. Spatial correlations of mantle structure with post-Archean geology permit

* Corresponding author.
E-mail address: alan.aitken@uwa.edu.au (A.R.A. Aitken).

https://doi.org/10.1016/j.gr.2022.11.016
1342-937X/

this controversy to be addressed and indicate that extensive mantle refertilisation occurred in the Proterozoic. Phases of lithospheric destabilisation are identified at ~ 2.06 and ~ 1.08 Ga, each associated with a significant magmatic event, while subsequent recratonisation is associated with the formation of sedimentary basins over 200–400 Ma. We highlight processes that favour the refertilisation of cratonic lithospheric mantle and its preservation during supercontinent assembly, with implications for tracking the growth of Earth's lithosphere through time.

2. The Yilgarn Craton - A crust-mantle dichotomy

The Yilgarn Craton (hereafter referred to as the craton) in Western Australia (Fig. 1) is an archetypal Archean craton, with geology characterised by greenstone belts dating from ca. 3.7 Ga to ca. 2.7 Ga, separated by Neoarchean granite domains dating from 2.68 to 2.62 Ga (Goscombe et al., 2019). The formation of the craton is inferred largely from the isotopic record of crust forming events (Champion and Cassidy, 2007; Mole et al., 2019). These studies define the growth of a geographically complete craton by the Neoarchean (Mole et al., 2019), and the establishment of a stable crustal architecture prior to the intrusion of the Widgiemooltha Dolerite at 2.42 Ga (Goscombe et al., 2019). Geophysical studies of bulk crustal properties also support an Archean crust formation (Yuan, 2015).

Geophysical studies of the lithospheric mantle resolve a substantially depleted composition: Mg/Fe ratios > 4.5 occur throughout west-central Australia (Khan et al., 2013), consistent with Mg# over 91. A 1D study for the entire West Australian Craton found bulk Mg# of ~ 91 – 91.5 and depletion in Al_2O_3 and CaO oxides (Qashqai et al., 2016). In a higher-resolution study (Fig. 2), regionally variable Mg# is estimated, on the base of a joint inversion of seismic and gravity models (Tesauro et al., 2020). A highly depleted western craton (Mg# > 90.5) contrasts with a typically less depleted eastern craton (Mg# < 90.5), including the Tropicana Zone of the Albany Fraser Orogen. The surrounding orogens and basins possess more fertile lithosphere (Mg# < 90.0). Although depleted relative to primitive mantle, the lithospheric mantle composition for much of the craton lies outside the range of xenolith data from

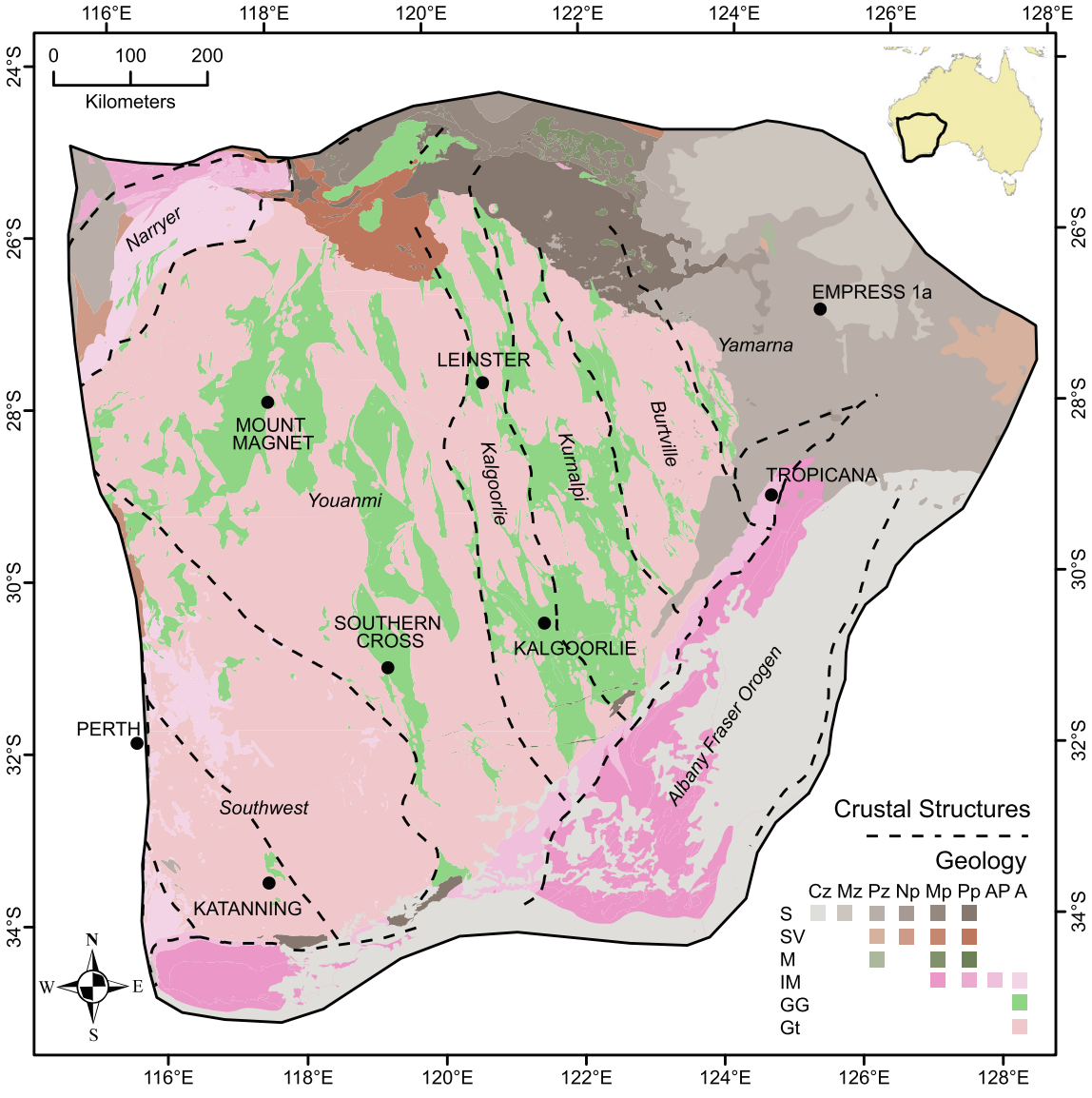

Fig. 1. Simplified geology of the Yilgarn Craton region. Major crustal structures (Korsch and Doublier, 2016), define zone boundaries (names in italics). Geology Legend: Cz – Cenozoic, Mz – Mesozoic, Pz – Paleozoic, Np – Neoproterozoic, Mp – Mesoproterozoic, Pp – Paleoproterozoic, AP –Archean-Paleoproterozoic, A - Archean; S – sedimentary, SV – sedimentary and volcanic, M – mafic igneous, IM – igneous and metamorphic, ISM – Igneous sedimentary and metamorphic, GG – greenstone belts, Gt – granite.

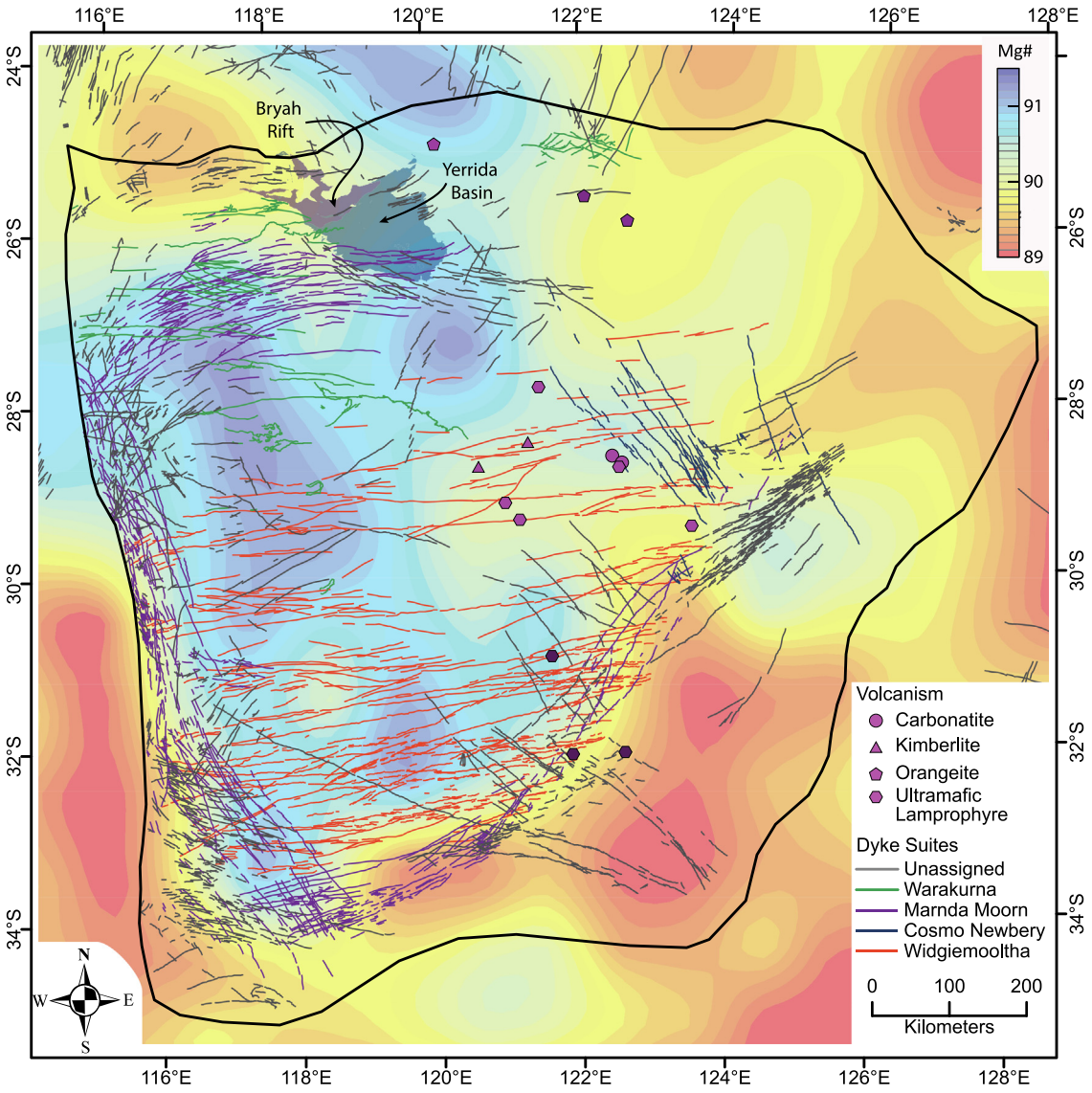

Fig. 2. Post-Archean magmatic events, showing the Yerrida Basin and Bryah Rift (2.18–2.01 Ga), major Proterozoic dyke suites. Boonadgin and Biberkine dyke suites (not shown) occur in the southwest (Stark et al., 2019). Alkaline magmatic rocks (Choi et al., 2020) are indicated with the central group at 2.06 Ga (bright shade), 1.8 to 1.4 Ga volcanism in the northern group (mid shade), and 0.86 Ga volcanism in the southern group (dark shade). The background image is modelled Mg# at 100 km depth (Tesauro et al., 2020). Inferred bulk mineral composition is shown in Fig. S1.

Archean regions (Griffin et al., 2008). This suggests refertilisation of the Archean lithosphere, causing increased density associated with higher iron content (Fig. 2), as well as higher proportion of clinopyroxene and garnet, with respect to olivine and orthopyroxene content (Griffin et al., 2003; Griffin et al., 2008; Tesauro et al., 2014) (Fig. S1).

For a fully-coupled crust and lithospheric mantle evolution, these key observations are mutually exclusive, and so they suggest a degree of decoupling in the evolution of the crust and mantle. To resolve this dichotomy, and to put constraints on the timing and mechanism of refertilisation, we review the craton's post-Archean geology and its lithosphere structure.

3. Post Archean geology of the Yilgarn Craton

Proterozoic rocks of the Yilgarn Craton are extensive, including dyke suites (Stark et al., 2019; Wingate, 2007), sedimentary basins (Grey et al., 2005; Occhipinti et al., 2017; Spaggiari et al., 2015), marginal metamorphic belts (Goscombe et al., 2019) and alkaline magmatic rocks (Choi et al., 2020; Fiorentini et al., 2020). Phanerozoic sedimentary basins also overlie the craton (Fig. 1). These post-Archean rocks, while volumetrically minor, are contemporaneous with globally significant tectonic events and may be subtle recorders of the developing cratonic lithosphere through time.

3.1. Surrounding orogenic belts

The exposed craton is surrounded by Proterozoic to Phanerozoic basins and Proterozoic orogens that have variably reworked the Archean crust. The Pinjarra Orogen to the west formed in-situ after ~ 1.1 Ga, with later events associated with the Cambrian Kuunga Orogen, and since the Permian the Perth Basin rifting (Markwitz et al., 2017). Besides detritus, currently there is no evidence of Archean heritage (Markwitz et al., 2017).

The Albany Fraser Orogen (AFO) represents the reworked southeast margin of the Yilgarn Craton (Kirkland et al., 2011), with major extension forming the Barren Basin from ca. 1.80 Ga to 1.31 Ga, and the Arid Basin from 1.60 to 1.31 Ga (Spaggiari et al., 2015). Later

contractional orogenesis occurred in two stages from 1.33 to 1.29 Ga and 1.23 to 1.14 Ga, with the Ragged Basin interstitial to these stages (Spaggiari et al., 2015). Post-Mesoproterozoic activity in the AFO is minimal (Scibiorski et al., 2016). The inboard AFO includes minimally reworked Yilgarn Craton crust in the Northern Foreland (Spaggiari et al., 2015) and the Tropicana Zone (Occhipinti et al., 2018). Terranes to the east of the AFO comprise Paleo-to Mesoproterozoic juvenile crust with no known Archean heritage (Spaggiari et al., 2015).

To the northeast, the west Musgrave Province formed as juvenile crust in the Proterozoic, with crust-forming events at ca 1.9 Ga, 1.62–1.55 Ga, 1.41 Ga and 1.34–1.29 Ga (Howard et al., 2015). The region was intensely reworked in an intraplate setting from 1.22 to 1.12 Ga (Smithies et al., 2011). Subsequently, and potentially as an extension of the preceding orogen (Smithies et al., 2015), the mafic–ultramafic dominated Giles Event magmatism occurred between 1.10 and 1.04 Ga, causing associated rifting (Aitken et al., 2013). The west Musgrave Province was partly overlain by the Neoproterozoic Officer and Amadeus basins before the onset of large-scale contractional deformation in the Ediacaran (Quentin de Gromard et al., 2019).

To the north, the Capricorn Orogen comprises several crustal blocks with multiple phases of amalgamation in the Paleoproterozoic. The Pilbara Craton, Yilgarn Craton and Glenburgh Terrane were combined by at least two events at ~ 2.2 Ga, and at ~ 2.0 G a (Johnson et al., 2011). The entire region was subsequently reworked during a prolonged series of intraplate tectonic events including at 1.82–1.77 Ga, 1.68–1.62 Ga, 1.39–1.20 Ga with more limited reworking at 1.03–0.95 Ga and in the late Neoproterozoic (Piechocka et al., 2018). In between these events basins formed including the 1.62–1.46 Ga Edmund Basin, and the 1.21–1.07 Ga Collier Basin (Johnson et al., 2013). The eastern Capricorn Orogen is overlain by the Neoproterozoic Officer Basin, and stratigraphic equivalents, while in the west the Mundine Well Dyke Suite was intruded at 0.75 Ga (Johnson et al., 2013). The southern Capricorn Orogen includes several regions of reworked Yilgarn Craton crust, including the Yarlarweelor Gneiss Complex and the Mary Mia Inlier (Fig. 3).

3.2. Yilgarn craton magmatic events

The Yilgarn Craton has experienced several large scale mafic magmatic events typified by dyke and sill intrusion. These include events at 2.42 Ga, 1.89 Ga, 1.39 Ga, 1.20 Ga, 1.08 Ga, and 0.75 Ga (Stark et al., 2019; Wingate, 2007). The 2.42 Ga Widgiemooltha Dolerite comprises prominent east-northeast striking dykes that extend across the craton for up to several hundred kilometres without significant deformation (Fig. 2). Notably, these dykes cross-cut the major crustal structures of the craton, providing a minimum bound on the age of the large-scale crustal architecture.

The 1.89 Ga Boonadgin and 1.39 Ga Biberkine dyke suites are known in the southwest Yilgarn Craton, where parallel arrays of dykes with east-southeast and south-southeast orientations are mapped (Stark et al., 2019). These dykes overly and are aligned with the edge of the high-velocity mantle of the Youanmi Terrane, suggesting that this lithospheric edge existed at 1.89 Ga, remained at 1.39 Ga and persists today. The 1.20 Ga Marnda-Moorn dyke swarm comprises several parallel arrays distributed around the highly-depleted core of the craton (Wang et al., 2014) suggesting that the northern, western and southeastern boundaries of the cratonic core were established by 1.2 Ga (Fig. 2).

Dykes and sills of the 1.08 Ga Warakurna LIP are extensive in the Collier and Salvation basins (Fig. 3), extending south into the craton (Wingate et al., 2004). Warakurna sills are prominent in seismic lines of the northern Youanmi Terrane, one example dated at 1070 ± 18 Ma (Wingate et al., 2008). Basalt in the Empress 1a core is dated at 1058 ± 13 Ma (Nelson, 1999). Tectonic reworking at ca 1.1 Ga is recognised at Agnew mine, with whole rock (1148 ± 23 Ma) and fine fraction (1094 ± 22 Ma) dates from extensional fault gouge (Thebaud and Zwingmann, 2012).

A range of alkaline magmatic rocks occur (Fig. 2), including 2.06 to 2.03 Ga ultramafic lamprophyres, kimberlites and carbonatites, 1.8 and 1.4 Ga orangeites, and 0.8 Ga ultramafic lamprophyres (Choi et al., 2020). The ca. 2.06 Ga event is interpreted to represent melting of sub-lithospheric mantle beneath the central Yilgarn Craton, whereas the orangeites are interpreted to represent melting of ancient enriched lithospheric mantle beneath the Earaheedy Basin (Choi et al., 2020). The emplacement of 0.8 Ga ultramafic lamprophyres in the southern Yilgarn Craton is interpreted to represent melting of a deep mantle source (Choi et al., 2020).

More voluminous magmatism is preserved only in the northern craton, where the Yerrida Basin experienced several phases of mafic magmatism during 2.18 to 2.01 Ga basin formation (Lindsay et al., 2020; Occhipinti et al., 2017). Mafic rocks in the lower Yerrida Basin plot in the OIB-array for TiO_2/Yb vs Nb/Yb, and possess negative $\Delta^{33}S$ signatures, indicating deep melting without an Archean signature. The magmatic volume emplaced is substantial, with a thickness of up to 2 km extending basin wide (Lindsay et al., 2020). By 2.04 Ga the Yerrida basin had transitioned to magma-dominated rifting including the Bryah sub-basin, this extending to 2.01 Ga (Occhipinti et al., 2017). Mafic rocks from the upper sequence plot in the MORB array for TiO_2/Yb vs Nb/Yb (Lindsay et al., 2020). The Bryah Rift preserves localised magmatic centres arranged en-echelon in the rift axis, with a mafic rock thickness of up to 6 km (Ramos et al., 2021). These characteristics suggest prior to 2.04 Ga an off-craton magmatic source, with more localised and shallow-sourced magmatism as the basin evolved to a narrow rift mode during the period 2.04 to 2.01 Ga.

3.3. Sedimentary basins

Post-Archean sedimentary rocks deposited over the craton, represent several main periods of subsidence. Paleoproterozoic basins developed around the northern, southern, and eastern margins of the craton in the period 2.18 – 1.69 Ga (Hall et al., 2008; Occhipinti et al., 2017). This period includes three phases, marked by transitional changes in basin character.

Phase-I is typified by the deposition of the lower Yerrida Basin beginning sometime after 2.18 Ga and evolving into a partial rift by 2.04 Ga (Occhipinti et al., 2017; Ramos et al., 2021). Deep-mantle sourced magmatism is contemporaneous with this phase both off-craton and on-craton (Choi et al., 2020; Lindsay et al., 2020). This phase ceases with the onset of the Glenburgh Orogeny at 2.00 Ga, with the Padbury Basin developing in the associated foreland (Occhipinti et al., 2017).

Phase- II involves broadly distributed sedimentation in the Earaheedy Basin and upper Yerrida Basin with two distinct subphases from 1.98 to 1.94 Ga and 1.89 to 1.82 Ga (Occhipinti et al., 2017; Rasmussen et al., 2012). This phase is characterised by a prolonged shallow marine transgression including carbonates, granular and banded iron formations and lacks major magmatism (Occhipinti et al., 2017). This phase ceased with the onset of the Capricorn Orogeny at 1.82 Ga, consistent with 1.86 to 1.84 Ga maximum deposition ages for the Earaheedy Basin (Hall et al., 2008) and 1843 ± 10 Ma monazite from the upper Yerrida Basin (Rasmussen and Fletcher, 2002). Apparently younger zircon ages from the upper Earaheedy Group (e.g. 1808 ± 36 Ma; 1796 ± 58 Ma (Halilovic et al., 2004)) have large errors and do not further constrain deposition. In the southern craton, the Stirling Range Formation was deposited in a marine setting between 2016 ± 6 Ma and 1800 ± 14 Ma Ga (Rasmussen et al., 2004). Although possibly younger than the northern basins, we consider

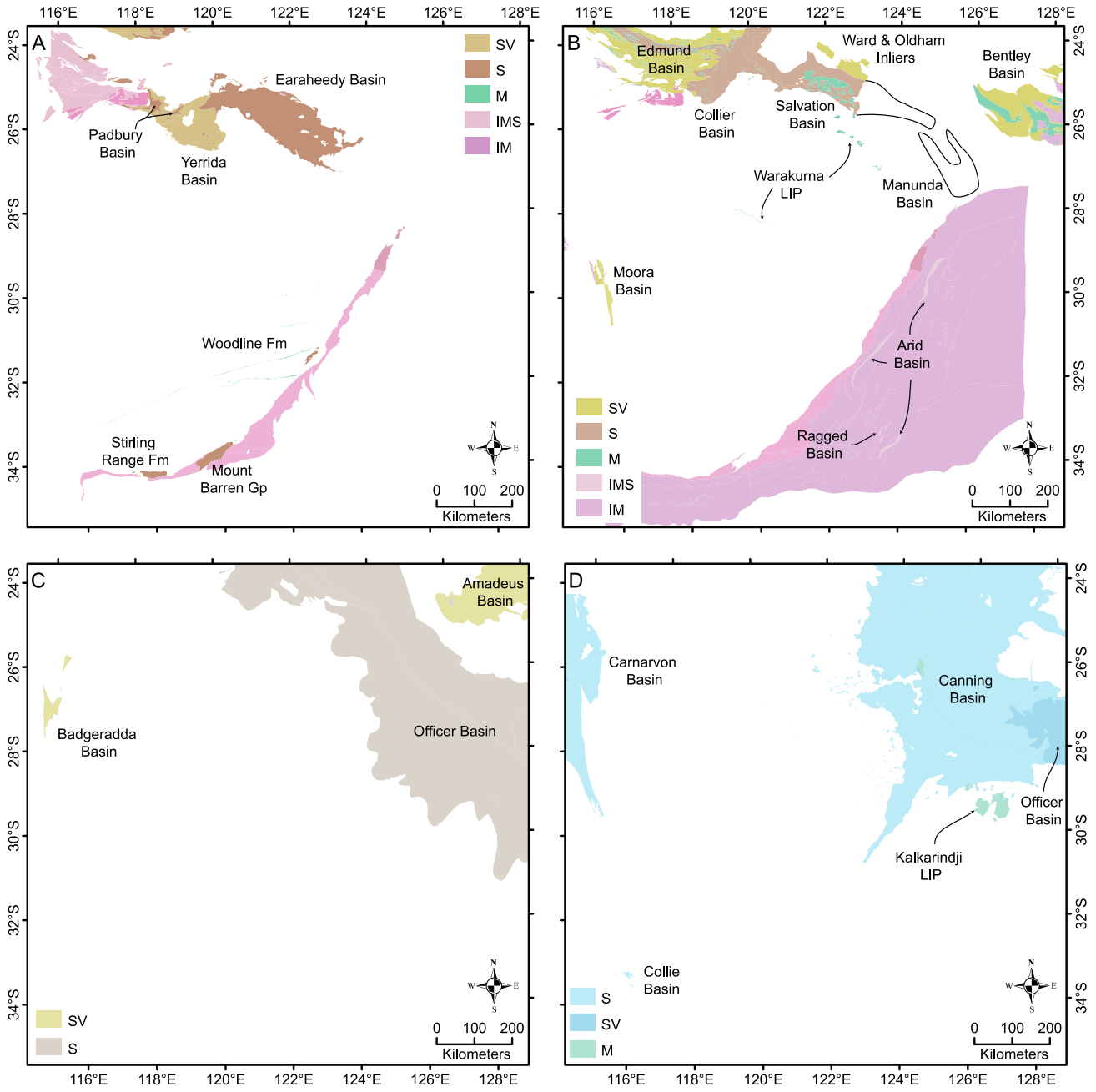

Fig. 3. Post-Archean geology of the Yilgarn Craton emphasising basin development a) Paleoproterozoic, b) Mesoproterozoic, c) Neoproterozoic, d) Paleozoic. Mesozoic and Cenozoic basins are shown in Fig. S2. Legend codes are as for Fig. 1.

it to belong to phase-II, as it is temporally distinct from phase-III basins.

With the exception of the Bryah sub-basin, the Phase-I and Phase-II basins overlie Archean crust that is undeformed at large scale, as indicated by continuity of underlying greenstone belts in magnetic and gravity data (Lindsay et al., 2020; Occhipinti et al., 2017). Phase-II is interpreted to represent craton-wide subsidence with basins forming as the craton is drawn down through sea level. The Earaheedy Basin has substantial peaks in detrital material at 2.6–2.8 Ga, 2.25 Ga, 2.04 Ga and 1.88 Ga (Hall et al., 2008). In contrast, the Stirling Range Formation a dominant population at 2.03 Ga (Rasmussen et al., 2004), with subordinate peaks at 2.6 Ga, 2.25 Ga, and none at 1.88 Ga. The difference in Neoarchean detritus may reflect the tilting of the craton, causing detritus eroded from the cratonic basement to be dominantly transported eastwards. Potential sources of the Paleoproterozoic detritus may include the Capricorn Orogen, volcanic rocks in the Yerrida Basin, or the upper portions of the alkaline volcanic system (Choi et al., 2020).

Phase-III includes the Barren Basin developed from 1.80 to 1.60 Ga (Spaggiari et al., 2015). Unlike the earlier basins, the Mount Barren Group overlies variably reworked crust marginal to the AFO. The Mount Barren Group preserves detrital populations of 2.6–2.8 and 2.03 Ga with approximately equal prevalence, with a more minor peak at 2.25 and a substantial population from 1.81 to 1.76 Ga (Hall et al., 2008). A maximum deposition age of ca 1.7 Ga (Hall et al., 2008) and a xenotime age of 1693 ± 4 Ma (Vallini et al., 2005) constrain Mount Barren Group deposition to ~ 100 Ma after the Stirling Range Formation. The Woodline Formation has similar detrital signature to the Earaheedy Group, being

dominated by 2.6–2.8 Ga detritus with minor peaks at 2.25, 2.03 and 1.89 Ga, the last including the youngest multi-grain population (Hall et al., 2008). The Woodline Formation has a single-grain maximum deposition age of 1737 ± 37 Ma (Hall et al., 2008), justifying its inclusion in phase-III, although otherwise it is consistent with phase-II.

Phase-III is interpreted to occur in response to changing tectonics at 1.82 to 1.65 Ga (Spaggiari et al., 2015), potentially due to the foundering of the craton edge. These smaller basins are evolving in association with coeval magmatism and extension and are distributed along the edge of the AFO, with metamorphosed equivalents also preserved within the orogen (Spaggiari et al., 2015). Phase-III may represent the influence of a new plate-margin developing to the southeast. This system evolves further in the Mesoproterozoic with the development of the 1.60 to 1.31 Ga Arid Basin, forming on highly extended Yilgarn Craton crust and the adjacent ocean crust (Spaggiari et al., 2015).

The second major period of basin forming begins with the deposition to the north of the craton of the late Mesoproterozoic Salvation and Collier basins, extending to ca. 1.07 Ga. Seismic and magnetic data define a contiguous basin overlying the northeastern Yilgarn Craton (Fig. 3), called the Manunda Basin (Korsch et al., 2013). These basins are heavily intruded by and closely associated with mafic rocks of the Warakurna LIP (Wingate et al., 2004), and this phase is interpreted to represent rifting of the northern craton boundary associated with the Giles Event.

In the Neoproterozoic the Officer Basin developed over the northeastern craton. The early phase of this basin sees a broad-scale basin forming, with the Buldya Group deposited in a northeast-deepening shelf (Grey et al., 2005). The basal Townsend Quartzite is not known to exist over the craton. The drillcore Empress 1A provides a relatively complete section from the Browne Formation upwards: in this record the maximum age of the Officer Basin sequence is derived from basalt in an underlying Mesoproterozoic sequence at 1058 ± 13 Ma. The Buldya Group sequence then comprises the evaporitic Browne Formation (840–818 Ma), the Hussar Formation (800 – 760 Ma), the Kanpa Formation (780 – 725 Ma) and the Steptoe Formation (<720 Ma). The core also preserves the diamictic Wahlgu Formation, correlated with the Marinoan glaciation. This sequence is capped by a basalt of the Table Hill Volcanics, dated at 484 ± 4 Ma. The development of the Neoproterozoic Officer Basin is traditionally interpreted to reflect a broad subsidence formed in relation to extension occuring during Rodinia breakup and linked to the intrusion of the Gairdner-Willouran LIP at 0.83 Ga (Walter et al., 1995), however, the craton preserves no evidence for Neoproterozoic rifting or substantial magmatism and mantle refertilisation of this age is not likely. The units deposited on-craton record the subsidence of the topographic surface through sea level between 0.85 and 0.70 Ga, while deeper basins developed in off-craton regions. We interpret the deposition of Neoproterozoic sediments on the craton to reflect ongoing plate cooling and subsidence following ~ 1.08 Ga refertilisation, augmented by a far-field response to off-craton rifting.

In the third period, the ca. 0.5 Ga Table Hill Volcanics, dominated by basalt, are overlain by clastic sedimentation and the partly glaciogenic Carboniferous-Permian Paterson Formation, which is relatively thin but widespread over central-Western Australia, including the Yilgarn Craton. The lower Permian Collie Subbasin (Perth Basin) is also deposited over the craton in the southwest. Apatite fission track analyses reflect gradual denudation of the craton since the Paleozoic, with a typical cooling age observed between 0.25 and 0.30 Ga, but with older cooling ages in the northeast, from 0.30 to 0.45 Ga (Gleadow et al., 2002). On detrital considerations, this cooling event has been interpreted to represent the removal of a broad sedimentary cover from the Yilgarn Craton, with relatively little denudation of the craton itself (Weber et al., 2005).

4. Lithospheric architecture

4.1. Seismic velocity structure

The seismic structure of the Yilgarn Craton lithospheric mantle is imaged in a number of seismic tomography studies as well as the AuSREM compilation (Fichtner et al., 2009, 2010; Fishwick and Rawlinson, 2012; Fishwick and Reading, 2008; Kennett et al., 2013; Yoshizawa, 2014; Yoshizawa and Kennett, 2015). These models resolve highly variable properties in the upper lithosphere but a less variable lower lithosphere.

A relatively homogenous lower lithosphere is resolved, with lithospheric thickness varying little except towards the south and southwest where the lithosphere has been thinned during Gondwana breakup. The southwest is characterised by a thinner and slower-velocity lithosphere, with moderate radial anisotropy. In the rest of the craton Vsv at 200 km depth lies in the range 4.71 ± 0.1 km/s (Fig. 4C) while models of seismic lithosphere thickness are consistently in the range 221 ± 6 km (Fig. S3). Co-variance of Vsv and lithospheric thickness suggest that temperature is the dominant control on the varying properties in the lower lithosphere. Radial anisotropy is distinctive, with low anisotropy in the west grading towards high anisotropy in the northeast (Fig. 4D). This is perhaps associated with the nature of the lithosphere-asthenosphere transition between Archean to heavily-modified Proterozoic lithosphere (Yoshizawa and Kennett, 2015).

In contrast to the lower lithosphere, the lithosphere above 125 km depth is more structured. Seismic wavespeed transitions from very fast in the west, with Vsv > 4.75 km/s at 100 km, to much slower in the east, with Vsv < 4.70 km/s (Fig. 4A). Radial anisotropy is the highest in the centre of the craton, lowest beneath the Earaheedy Basin, and generally lower in the west than the east (Fig. 4B). The velocity structures observed at this depth cannot readily be explained by temperature variations alone and must also represent major changes in mantle composition (Fichtner et al., 2010; Fishwick and Reading, 2008; Kennett et al., 2013).

The variations in seismic velocity structure allow the definition of three fundamentally different lithosphere types with differing compositional layering. Velocity gradients are less sensitive to temperature differences than velocity and distinguishes these types for the craton (Fig. 5). Type-1 lithosphere has a very high velocity, low-attenuation, low Vp/Vs and an almost radially isotropic upper layer, with a negative velocity gradient (ΔVsv < -0.5 km/s). Type 2 lithosphere is associated with a distinct transition towards reduced velocity in the upper lithosphere, with corresponding increases in attenuation and Vp/Vs (Fig. S4), but with relatively neutral velocity gradient (-0.5 < ΔVsv < 0.5 km/s). The boundary between type-1 and type-2 lithosphere is marked by high radial anisotropy for 200–300 km to its east (Fig. 4D). Finally in the northeast, type-3 lithosphere has a characteristically low velocity upper lithosphere, with corresponding high attenuation and Vp/Vs (Fig. S4), and positive velocity gradient (ΔVsv > 0.5 km/s), with moderate radial anisotropy in the upper lithosphere (Fig. 4B).

4.2. Reconciliation with surface geology

Clear associations exist between the lithospheric architecture and surface geology, including the Archean structure, as well as Proterozoic igneous and sedimentary rocks and Paleozoic sedimen-

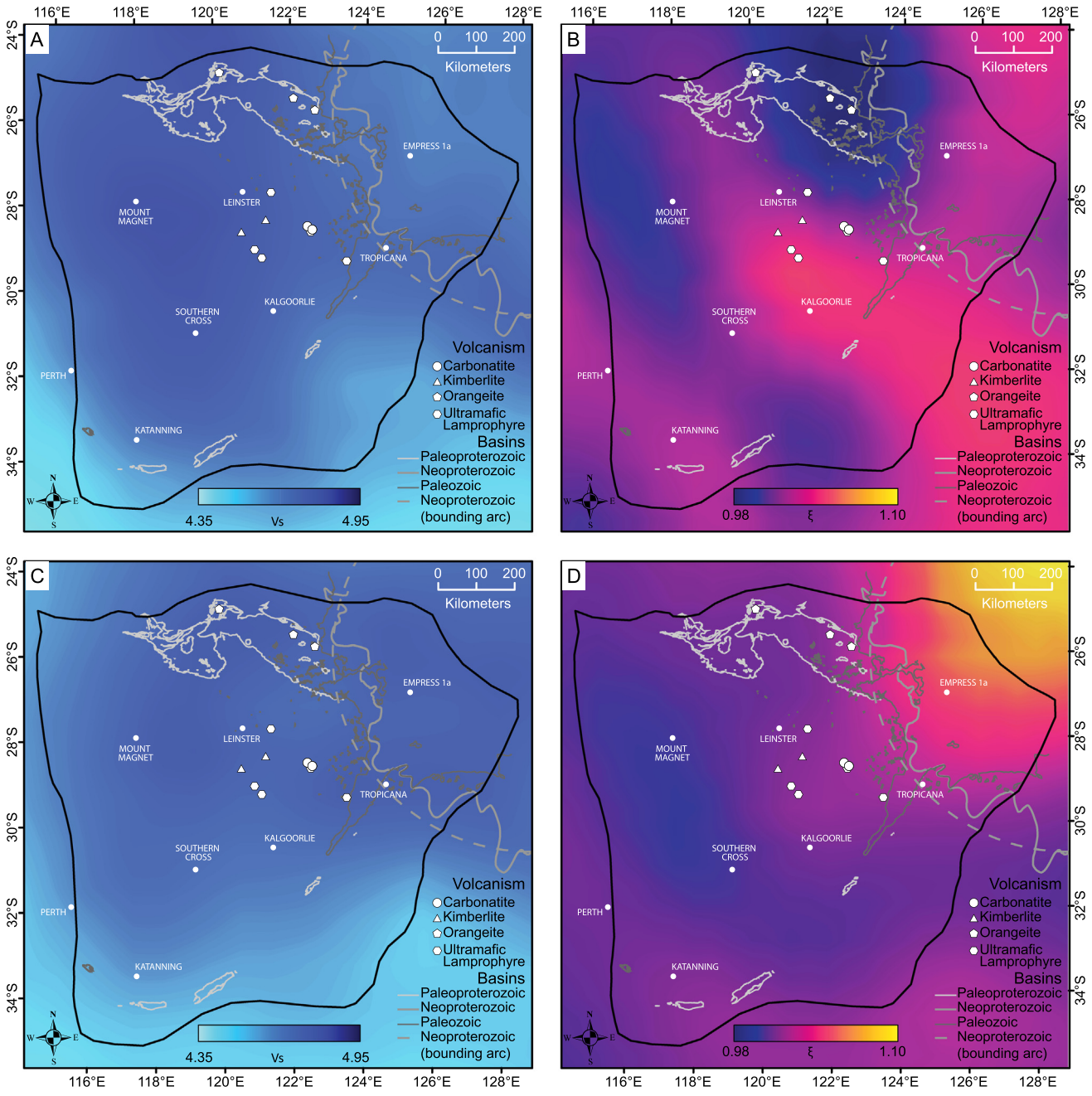

Fig. 4. Mantle seismic properties a) AuSREM Vsv (Kennett et al., 2013) at 100 km depth b) radial anisotropy at 100 km depth (Yoshizawa, 2014) c), d) as a), b) at 200 km depth. Selected volcanic suites and basin outlines are shown. Additional Vsv and Vsh from these models are shown in Fig. S3, and further properties from AuSREM are shown for the seven named sites in Fig. S4.

tary rocks. Type-1 lithosphere includes most of the Youanmi and southwest Terranes and defines the relatively less modified cratonic core. Post-Archean geology includes dykes and sills from several magmatic events (Wingate, 2007) but currently no evidence exists for volcanic or sedimentary rocks. Paleozoic sedimentary rocks are also absent from the Type-1 lithosphere. For this region we suggest a well-preserved Archean upper lithosphere overlies a more fertile lower lithosphere, likely of Proterozoic origin.

Type-2 lithosphere includes most of the Kalgoorlie, Kurnalpi and Burtville Terranes, the Paleoproterozoic Yerrida and Earaheedy basins, and the western edge of the craton. Paleoproterozoic sedimentary rocks occur widely over type-2 lithosphere including the Yerrida and Earaheedy Basins and the Stirling Range Formation (Fig. 5). Small outcrops of Paleozoic sedimentary rocks, while sparse, are present throughout (Fig. 5). Paleoproterozoic mafic magmatic rocks emplaced between 2.2 and 2.0 Ga are found only within type-2 lithosphere, and are focused in a ~ 250 km wide corridor immediately east of the boundary with type-1 lithosphere (Fig. 5). This corridor is associated with high radial anisotropy (Fig. 4B) and increased fertility relative to type 1 lithosphere (Fig. 2). Further east, the amagmatic Earaheedy Basin is associated with low radial anisotropy in the upper lithosphere, but has the higher fertility mantle and neutral velocity gradient consistent with type-2 lithosphere (Fig. 2). Later Proterozoic orangeites here represent melting of ancient enriched lithospheric mantle (Choi et al., 2020). For type-2 lithosphere we propose that the entire lithosphere was substantially refertilised during the Paleoproterozoic.

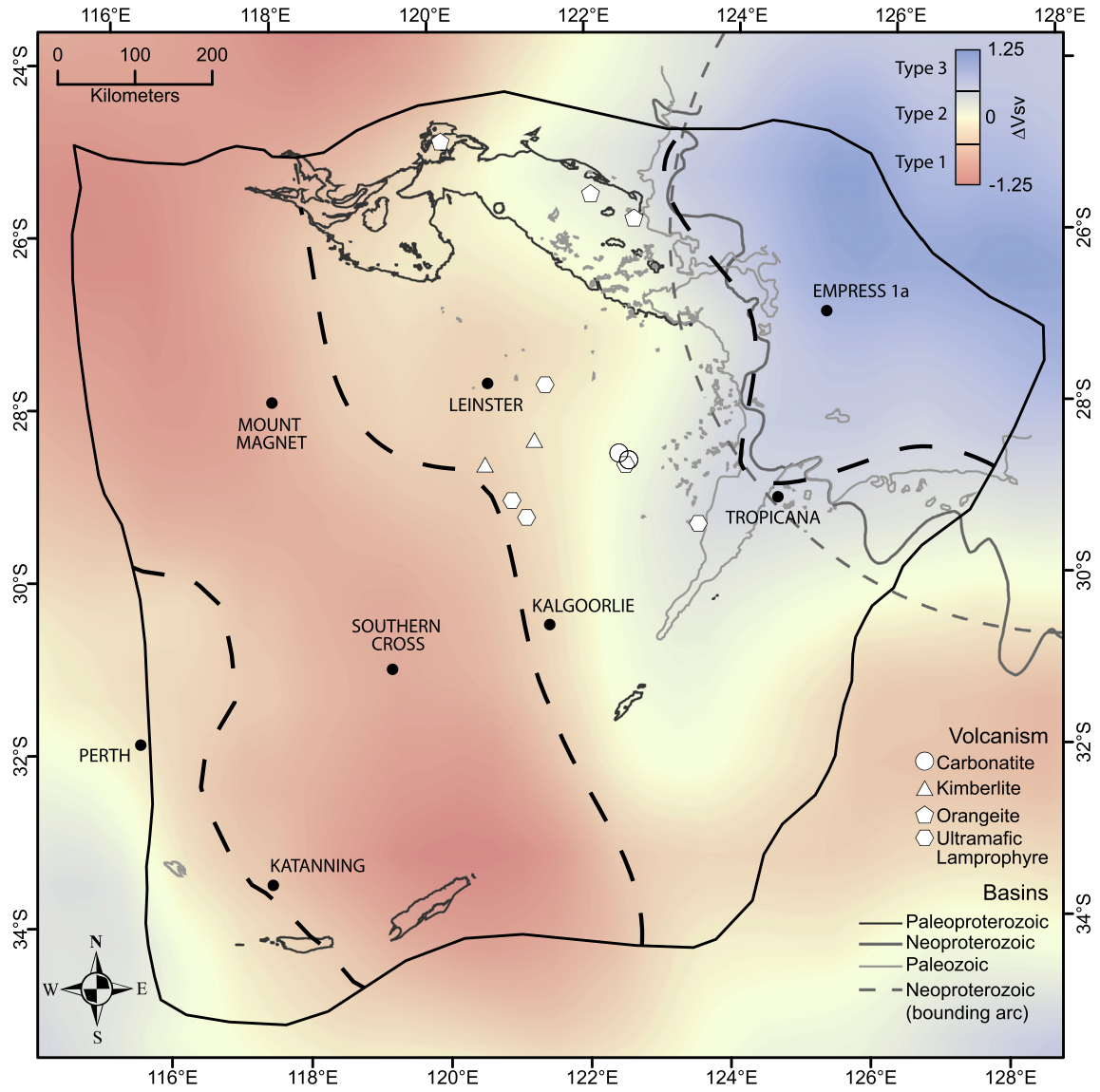

Fig. 5. Layered seismic lithospheric structure derived from AuSREM (Kennett et al., 2013) showing ΔVsv (km/s) between 200 and 100 km depth (see Fig. 4A,C). There are also displayed selected volcanic suites and basin outlines. Heavy dashed lines indicate boundaries between interpreted lithosphere types.

The edge of Neoproterozoic basin cover delineates, for over 1000 km, the arc of a circle of diameter 1030 km, centred in the west Musgrave Province (Fig. 5) and is coincident with the type-3 lithosphere. This region is also closely associated with the existence of magmatic rocks of the Warakurna LIP and Giles Event (Wingate et al., 2004) and its magmatic underplate (Alghamdi et al., 2018). In addition, Paleozoic sedimentary rocks are near-continuous over the type-3 lithosphere (Fig. 3D). Previous studies have interpreted a possible pargasitic phase in this region linked to Proterozoic intraplate reworking (Fishwick and Reading, 2008). For type 3 lithosphere we interpret the low-velocity upper lithosphere to represent partly increased temperature from thermal blanketing, but also strong compositional changes from refertilisation processes. The highly anisotropic lower mantle may also be representative of a large degree of Proterozoic reworking (Yoshizawa and Kennett, 2015).

5. Multi-stage evolution of the Yilgarn Craton mantle

Lithosphere architecture applies a first-order control on the development of crustal geology and surface processes. A necessary consequence of mantle refertilisation is increased density, which notwithstanding compensating changes in crustal structure or lithospheric thickness, eventually causes subsidence (Wenker and Beaumont, 2018). Initially, the topographic surface may be supported by thermal buoyancy, and commonly there will be a lag in subsidence. However as the thermal buoyancy slowly wanes, prolonged subsidence occurs extending over tens to hundreds of million years (Eaton and Claire Perry, 2013). As the topographic surface is drawn down, sediment deposition may occur. In particular, a slow drawdown through sea-level may cause a prolonged marine transgression. The combination of a magmatic-dominated 'rift' event followed by prolonged deposition of sag-type sedimentary basins over the undeformed craton is a clear indicator of mantle refertilisation. With this in mind, the following evolution for the Yilgarn Craton is proposed.

5.1. Stage I – Archean formation of the cratonic lithosphere

The Archean evolution of the crust is mapped in some detail from isotopic systems (Mole et al., 2019), and in bulk crustal properties (Yuan, 2015). A series of crustal growth events is resolved between 3.2 and 2.6 Ga, with the Youanmi and Burtville Terrane crust forming prior to 2.8 Ga, and the youngest crust-forming events occurring at 2.7 Ga in the Kalgoorlie and Kurnalpi Terranes (Mole et al., 2019), with mantle melting extending into the latest Archean (Choi et al., 2020). From the crustal evolution we infer that a continental lithospheric mantle was formed under the entire craton by the end of the Archean (Fig. 6). The preserved crust and high-velocity upper lithospheric layer of type-1 lithosphere indicates at least a 100 to 150 km thick lithosphere, potentially with thinner lithosphere under the Kalgoorlie and Kurnalpi Terranes due to Neoarchean rifting (Mole et al., 2019).

5.2. Stage II – Paleoproterozoic modification of the central Yilgarn Craton

Widgiemooltha Dolerite dykes intruded craton-wide at 2.42 Ga and remain in a largely undeformed state. Although with a large magma volume, the lack of subsequent basins suggest this was not a refertilisation event. The period between 2.18 and 2.01 Ga is associated with magmatic-dominated basin development in the Yerrida Basin as well as alkaline intrusive magmatism in the eastern craton (Choi et al., 2020; Fiorentini et al., 2020). All these mafic magmatic rocks sit on type-2 lithosphere focused in a zone < 250 km wide immediately east of the edge of the high-

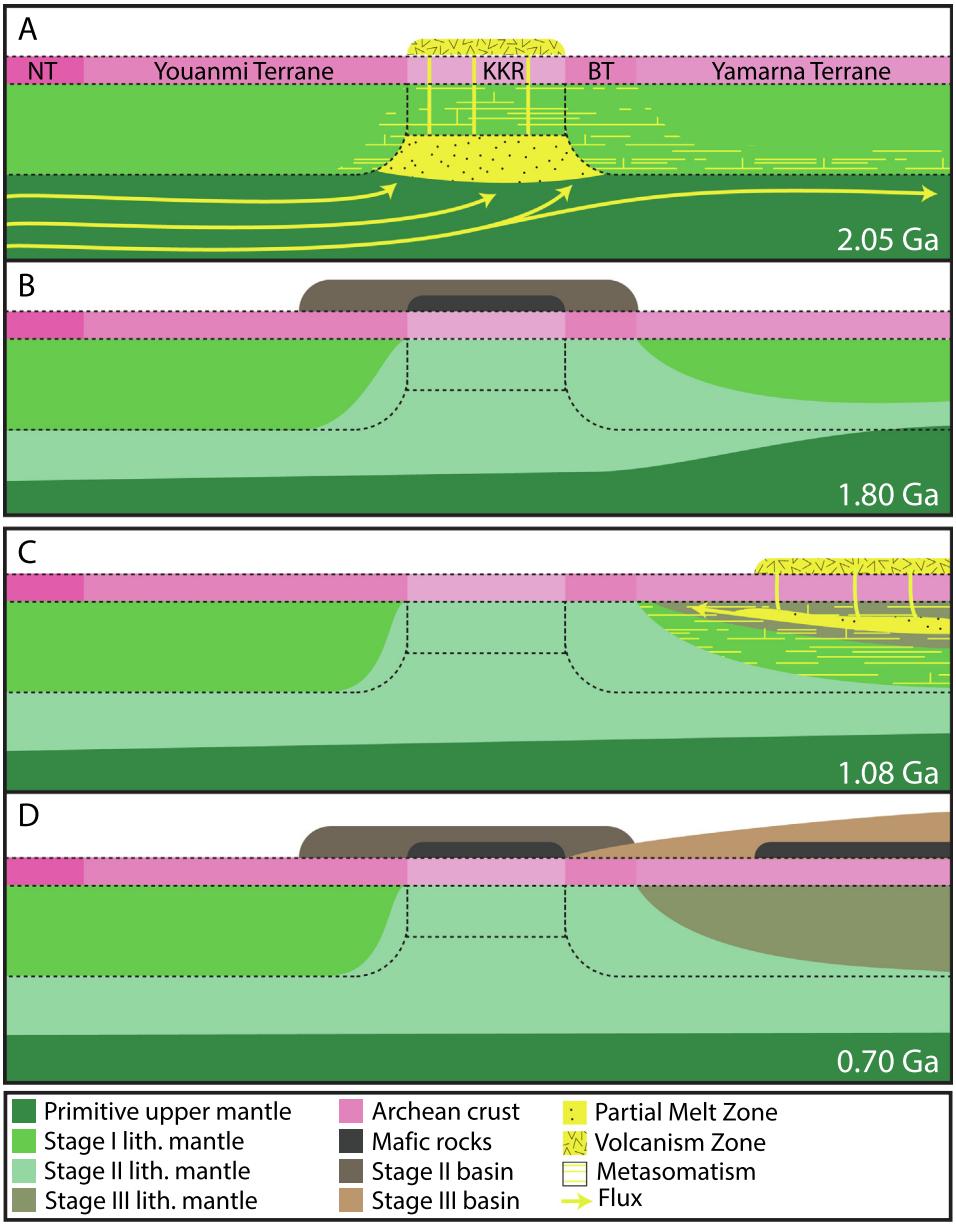

Fig. 6. Cartoon of magmatic destabilisation and recratonisation for the northern Yilgarn Craton showing a) Stage II lithosphere refertilisation at ~ 2.06 Ga due to mantle flow from the north-west, b) the recratonisation and formation of basins by 1.80 Ga, c) Stage III incursion of fertile mantle forming type-3 lithosphere structure at ~ 1.08 Ga with recratonisation and d) formation of basins by ~ 0.70 Ga. Dashed lines indicate the inferred Archean lithosphere from stage I. KKR – Kalgoorlie-Kurnalpi Rift BT – Burtville Terrane. Supracrustal rock packages are not to scale.

velocity upper lithosphere (Fig. 5). A preceding model for the alkaline intrusive rocks has linked their genesis to the contemporaneous Bushveld Igneous Complex plume (Fiorentini et al., 2020). Numerical modelling demonstrates such a connection is physically possible given a suitable paleogeography (Fiorentini et al., 2020).

Regardless of the link to broader magmatic events, Yilgarn Craton magmatism in this period represents the effect of a major sub-lithospheric mantle flow, migrating from the northwest. We suggest that south-east directed flow crosses a lithospheric step at the edge of the Youanmi Terrane, causing shear-induced edge-driven convection (Kaislaniemi and van Hunen, 2014) and associated sub-lithospheric melting and magmatism in the lee of this feature.

Exposed peridotite massifs around the world provide insights into the nature of metasomatic processes occurring in the lithospheric mantle, with the injection of pyroxene-rich and olivine-poor melt as networks of veins (Bodinier et al., 2008; Mazzucchelli et al., 2008). Although compositionally distinct, these veins make up a small-volume of the bulk rock, lowering the melting point of localised domains of the lithospheric mantle and controlling the chemical composition of alkali-rich melts derived from their fusion (Holwell et al., 2019). Over the large spatially-averaged volumes to which geophysical data are sensitive, these localised compositional variations generate regional changes in bulk composition. High radial anisotropy supports a horizontally-layered velocity structure at small scales, consistent with observations in peridotite massifs (Bodinier et al., 2008; Mazzucchelli et al., 2008).

The refertilisation of the type-2 lithosphere is proposed to have generated ongoing craton-wide subsidence over the subsequent ~ 250 Ma, with sediments deposited as the surface was drawn down through sea level. The negative buoyancy of the eastern craton, relative to the western craton, may have tilted the topographic surface, directing detritus dominantly towards the east. From 1.8 Ga, changing tectonics in central Australia may have caused the vulnerable southeastern edge of the craton to collapse, leading to the formation of the Barren Basin.

5.3. Stage III – meso- to Neoproterozoic modification of the north-eastern Yilgarn Craton

Late Mesoproterozoic tectonics in the west Musgrave Province led to a very thin lithosphere, as a consequence of a series of lithospheric delaminations (Gorczyk et al., 2015; Smithies et al., 2015). By this means the northeastern edge of the Yilgarn Craton at ~ 1. 1 Ga was exposed to instability, leading to the development of Collier, Salvation and Manunda Basins and also extensional brittle fracturing in the northern craton (Thebaud and Zwingmann, 2012). We propose that, as the 1.08 Ga Giles Event impinged on this lithosphere, a subcrustal extrusion of fertile mantle emanated beneath the craton from a source region beneath the west Musgrave Province. Extrusion of fertile mantle was accompanied by magmatism and emplacement of a crustal underplate and the upper lithospheric mantle was thickened and extensively refertilised.

Anomalous lithospheric mantle underlies all the major depocentres of the Neoproterozoic Centralian Superbasin, suggesting a broadly impactful event (Fichtner et al., 2010; Fishwick and Reading, 2008; Tesauro et al., 2020). Initially the surface was elevated, supported by a thick and buoyant crust and hot mantle, with early units of the Officer Basin reflecting the erosion of volcanic highlands (Walter et al., 1995); however, as the lithospheric mantle cooled, subsidence led to the deposition of the Officer Basin over the north-eastern margin of the craton between 0.85 and 0.70 Ga. The onset of crustal extension to the east associated with Rodinia breakup from ~ 0.83 Ga likely enhanced this subsidence.

The boundaries of Neoproterozoic and Paleozoic basins are co-located (Fig. 5) and it is possible that the Cambrian Table Hill Volcanic event (Kalkarindji LIP) may also be associated with renewed basin formation extending into the Permian. Although a valid candidate event for refertilisation, the magnitude of this event is much less than the Giles Event, and the overlying basin is much thinner. Paleozoic rocks are widespread, albeit sparse, across the Type-2 lithosphere.

6. Controls on magmatic destabilisation and recratonisation in supercontinent evolution

The evidence for multiple phases of refertilisation of the Yilgarn Craton lithospheric mantle, preserved in distinct lithospheric domains, is reconciled with the extents of magmatic events at 2.06 Ga and at 1.08 Ga. Each of these magmatic events precedes a prolonged period of basin formation that is interpreted to reflect subsidence caused by the dense refertilised mantle, subject to a thermal relaxation time lag, and modulated by ongoing tectonics in the surrounding regions. These magmatic events occurred during phases of increasing craton collision frequency in the build-up to fully assembled supercontinents (Condie et al., 2015). For a more general view, we may seek to understand the potential for systematic controls linked to this phase of the supercontinent cycle.

The proposed refertilisation events are coeval with two of Earth's largest mafic/ultramafic magmatic events, and specifically events characterised by large-volume layered intrusions emplaced into the upper crust. Magmatism at ~ 2.06 Ga is contemporaneous with the Bushveld Igneous Complex, while magmatism at 1.08 Ga is linked to the Giles Event. With respect to the Yilgarn Craton, these major events are differently located (distal vs proximal) and have different geodynamic origins (plume vs non-plume). Rather than a relationship with a specific geodynamic setting, a more general relationship is suggested between high magma flux, extensive regional modification of the lithosphere and preservation of these to the present day.

Destabilisation requires sufficient magma flux to refertilise large volumes of mantle. The required rates of vertical magma flux needed for destabilisation exceed those typical of mid-ocean ridges and in rifts and arcs; however, the emplacement of a LIP may readily exceed this (Wenker and Beaumont, 2018). For LIPs, although there is no clear co-cyclicity with the supercontinent cycle, there is an apparent increase in LIP frequency in the periods of increased collision rate preceding assembly (Condie et al., 2015). This observation includes the effect of preservation. For the Yilgarn Craton, it is apparent that refertilisation is associated with mantle-flux migrating beneath the craton from off-craton magmatic centres, which is dependent on the geodynamic setting.

Upwelling hot mantle may cause thermal erosion (Xu, 2001) topographic swells and superswells (McNutt, 1998), and lateral mantle flow may exert a divergent traction on the base of the lithosphere (Koptev et al., 2015; Zhang et al., 2018), so generating lithospheric extension. Under far-field tension, upwelling-induced and tectonic stresses share sign, and where these exceed the strength of the lithosphere, these processes may rapidly lead to breakup and plate dispersal (Buiter and Torsvik, 2014; Huang et al., 2019; Wenker and Beaumont, 2018; Yoshida, 2010). In such a scenario, mantle refertilisation will be focused toward the edges of the newly formed tectonic plates. These margins are susceptible to gravitational instability, as well as destruction in later collisions (Wang et al., 2018). In contrast, in a sufficiently non-tensile setting, where magmatic and tectonic stresses combined do not exceed lithospheric strength, lithospheric extension and vertical magma

transport will be inhibited, favouring enhanced lateral flow. The Giles Event, for example, occurred in a generally compressive setting, with extension due to magmatic loading, but also is characterised by the emplacement of an extensive crustal underplate and net crustal thickening (Aitken et al., 2013).

Models of the late stages of supercontinents show subplanetary scale mantle convection, including upwelling beneath the supercontinent, and dominant tension in the supercontinent (Dal Zilio et al., 2018; Mitchell et al., 2021; Zhang et al., 2018). In contrast, in models of the assembling supercontinent stage, planetary-scale mantle convection draws continental elements together over a single 'superdownwelling' (Mitchell et al., 2021; Yoshida and Santosh, 2011; Zhong et al., 2007). In this phase a compressional to neutral stress-field occurs, as plates assemble above the mantle downwelling (Gurnis, 1988). Furthermore, post-assembly, a stable intracontinental setting allows gradual cooling and recratonisation to occur over 200–400 Ma (Eaton and Claire Perry, 2013) favouring long-term preservation of the refertilised lithosphere in an intraplate setting, protected from gravitational instability and from later collisions. Thus, we argue that while the amount of refertilisation occurring during supercontinent breakup phases is undoubtedly substantial, this refertilised lithosphere is focused at the newly forming plate margins and is more likely to later be recycled into the mantle. We consider that refertilisation occurring during supercontinent assembly phase has the potential to penetrate further beneath cratonic regions and that resulting refertilisation has a much higher preservation potential.

7. Conclusion

Magmatic destabilisation of the mantle and its recratonisation are key processes in craton evolution that are not always recognised in datasets recording crustal isotopic evolution, which may carry strong preservation bias (Mulder and Cawood, 2021). Such events can be detected however through geophysical recognition of fertile mantle compositions, spatially associated with magmatic events, and the later formation of broad sedimentary basins over unrifted crust. For the Yilgarn Craton, such episodes occurred at $\sim$ 2.06 and $\sim$ 1.08 Ga, suggesting an association with the early stages of supercontinent assembly. A general significance cannot be assumed from this example, however, a similar pattern is seen in the North Atlantic Craton, which saw refertilisation associated with alkaline magmatic rocks emplaced at 1.4–1.2 Ga and at $\sim$ 0.6 Ga, each preceding basin formation and rifting episodes, but through which the craton remained intact, before finally succumbing to lithospheric thinning and breakup in the late Mesozoic-Cenozoic (Tappe et al., 2007).

Key linkages between the geodynamics of supercontinent assembly and large-volume magmatic events may favour the occurrence of widespread destabilisation and refertilisation, crucially avoiding lithospheric failure and breakup. The geodynamic stability of the assembled supercontinent allows subsequent recratonisation in a continental interior, so protecting the refertilised lithosphere from later events. Consequently, we suggest the post-Archean development of cratonic lithosphere is predisposed towards preserving refertilisation occurring during periods of supercontinent assembly and these periods are potentially dominant over periods of supercontinent dispersal.

CRediT authorship contribution statement

A.R.A. Aitken: Conceptualization, Methodology, Investigation, Writing – original draft, Project administration, Funding acquisition. **M. Fiorentini:** Conceptualization, Writing – original draft, Funding acquisition. **M. Tesauro:** Methodology, Investigation, Writing – original draft. **N. Thébaud:** Conceptualization, Writing – original draft, Project administration, Funding acquisition.

Declaration of Competing Interest

The authors declare that they have no known competing financial interests or personal relationships that could have appeared to influence the work reported in this paper.

Acknowledgements

This research was supported by the Yilgarn 2020 project funded by the Minerals Research Institute of Western Australia (Project M530) and industry sponsors. We thank Kazunori Yoshizawa for supplying his tomography models.

Appendix A. Supplementary material

Supplementary data to this article can be found online at https://doi.org/10.1016/j.gr.2022.11.016.

References

Afonso, J., Ben Mansour, W., O'Reilly, S., Griffin, W., Salajegheh, F., Foley, S., Begg, G., Selway, K., Macdonald, A., Januszczak, N., Fomin, I., Nyblade, A., Yang, Y., 2021. Thermochemical structure and evolution of cratonic lithosphere in central and southern Africa.

Aitken, A.R.A., Smithies, R.H., Dentith, M.C., Joly, A., Evans, S., Howard, H.M., 2013. Magmatism-dominated intracontinental rifting in the Mesoproterozoic: The Ngaanyatjarra Rift, central Australia. Gondw. Res. 24, 886–901.

Alghamdi, A.H., Aitken, A.R.A., Dentith, M.C., 2018. The deep crustal structure of the Warakurna LIP, and insights on Proterozoic LIP processes and mineralisation. Gondw. Res. 56, 1–11.

Bodinier, J.-L., Garrido, C.J., Chanefo, I., Bruguier, O., Gervilla, F., 2008. Origin of Pyroxenite-Peridotite Veined Mantle by Refertilization Reactions: Evidence from the Ronda Peridotite (Southern Spain). J. Petrol. 49, 999–1025.

Buiter, S.J.H., Torsvik, T.H., 2014. A review of Wilson Cycle plate margins: A role for mantle plumes in continental break-up along sutures? Gondw. Res. 26, 627–653.

Champion, D., Cassidy, K., 2007. An overview of the Yilgarn Craton and its crustal evolution. Geoscience Australia Record 14, 8–13.

Choi, E., Fiorentini, M.L., Hughes, H.S.R., Giuliani, A., 2020. Platinum-group element and Au geochemistry of Late Archean to Proterozoic calc-alkaline and alkaline magmas in the Yilgarn Craton, Western Australia. Lithos 374–375, 105716.

Condie, K.C., Davaille, A., Aster, R.C., Arndt, N., 2015. Upstairs-downstairs: supercontinents and large igneous provinces, are they related? Int. Geol. Rev. 57, 1341–1348.

Dal Zilio, L., Faccenda, M., Capitanio, F., 2018. The role of deep subduction in supercontinent breakup. Tectonophysics 746, 312–324.

Eaton, D.W., Claire Perry, H.K., 2013. Ephemeral isopycnicity of cratonic mantle keels. Nat. Geosci. 6, 967–970.

Fichtner, A., Kennett, B.L.N., Igel, H., Bunge, H.P., 2009. Full seismic waveform tomography for upper-mantle structure in the Australasian region using adjoint methods. Geophys. J. Int. 179, 1703–1725.

Fichtner, A., Kennett, B.L.N., Igel, H., Bunge, H.P., 2010. Full waveform tomography for radially anisotropic structure: New insights into present and past states of the Australasian upper mantle. Earth Planet. Sci. Lett. 290, 270–280.

Finger, N.-P., Kaban, M.K., Tesauro, M., Mooney, W.D., Thomas, M., 2022. A Thermo-Compositional Model of the African Cratonic Lithosphere. Geochem. Geophys. Geosyst. 23. e2021GC010296.

Fiorentini, M.L., O'Neill, C., Giuliani, A., Choi, E., Maas, R., Pirajno, F., Foley, S., 2020. Bushveld superplume drove Proterozoic magmatism and metallogenesis in Australia. Sci. Rep. 10, 19729.

Fishwick, S., Rawlinson, N., 2012. 3-D structure of the Australian lithosphere from evolving seismic datasets. Aust. J. Earth Sci. 59, 809–826.

Fishwick, S., Reading, A.M., 2008. Anomalous lithosphere beneath the Proterozoic of western and central Australia: A record of continental collision and intraplate deformation? Precambr. Res. 166, 111–121.

Gleadow, A.J.W., Kohn, B.P., Brown, R.W., O'Sullivan, P.B., Raza, A., 2002. Fission track thermotectonic imaging of the Australian continent. Tectonophysics 349, 5–21.

Gorczyk, W., Smithies, H., Korhonen, F., Howard, H., Quentin De Gromard, R., 2015. Ultra-hot Mesoproterozoic evolution of intracontinental central Australia. Geosci. Front. 6, 23–37.

Goscombe, B., Foster, D.A., Blewett, R., Czarnota, K., Wade, B., Groenewald, B., Gray, D., 2019. Neoarchaean metamorphic evolution of the Yilgarn Craton: A record of

subduction, accretion, extension and lithospheric delamination. Precambr. Res. 335, 105441.
Grey, K., Hocking, R., Stevens, M., Bagas, L., Carlsen, G., Irimies, F., Pirajno, F., Haines, P., Apak, S., 2005. Lithostratigraphic Nomenclature of the Officer Basin and Correlative Parts of the Paterson Orogen, Western Australia.
Griffin, W.L., O'Reilly, S.Y., Abe, N., Aulbach, S., Davies, R.M., Pearson, N.J., Doyle, B.J., Kivi, K., 2003. The origin and evolution of Archean lithospheric mantle. Precambr. Res. 127, 19–41.
Griffin, W.L., O'Reilly, S.Y., Afonso, J.C., Begg, G.C., 2008. The Composition and Evolution of Lithospheric Mantle: a Re-evaluation and its Tectonic Implications. J. Petrol. 50, 1185–1204.
Gurnis, M., 1988. Large-scale mantle convection and the aggregation and dispersal of supercontinents. Nature 332, 695–699.
Halilovic, J., Cawood, P.A., Jones, J.A., Pirajno, F., Nemchin, A.A., 2004. Provenance of the Earaheedy Basin: implications for assembly of the Western Australian Craton. Precambr. Res. 128, 343–366.
Hall, C.E., Jones, S.A., Bodorkos, S., 2008. Sedimentology, structure and SHRIMP zircon provenance of the Woodline Formation, Western Australia: Implications for the tectonic setting of the West Australian Craton during the Paleoproterozoic. Precambr. Res. 162, 577–598.
Hoggard, M.J., Czarnota, K., Richards, F.D., Huston, D.L., Jaques, A.L., Ghelichkhan, S., 2020. Global distribution of sediment-hosted metals controlled by craton edge stability. Nat. Geosci. 13, 504–510.
Holwell, D.A., Fiorentini, M., McDonald, I., Lu, Y., Giuliani, A., Smith, D.J., Keith, M., Locmelis, M., 2019. A metasomatized lithospheric mantle control on the metallogenic signature of post-subduction magmatism. Nat. Commun. 10, 3511.
Howard, H.M., Smithies, R.H., Kirkland, C.L., Kelsey, D.E., Aitken, A., Wingate, M.T.D., De Gromard, R.Q., Spaggiari, C.V., Maier, W.D., 2015. The burning heart—the Proterozoic geology and geological evolution of the west Musgrave Region, central Australia. Gondw. Res. 27, 64–94.
Huang, C., Zhang, N., Li, Z.X., Ding, M., Dang, Z., Pourteau, A., Zhong, S., 2019. Modeling the Inception of Supercontinent Breakup: Stress State and the Importance of Orogens. Geochem. Geophys. Geosyst. 20, 4830–4848.
Huang, J., Zhao, D., Zheng, S., 2002. Lithospheric structure and its relationship to seismic and volcanic activity in southwest China. Journal of Geophysical Research: Solid Earth 107, ESE 13-11-ESE 13-14.
Johnson, S.P., Sheppard, S., Rasmussen, B., Wingate, M.T.D., Kirkland, C.L., Muhling, J. R., Fletcher, I.R., Belousova, E.A., 2011. Two collisions, two sutures: Punctuated pre-1950Ma assembly of the West Australian Craton during the Ophthalmian and Glenburgh Orogenies. Precambr. Res. 189, 239–262.
Johnson, S.P., Thorne, A.M., Tyler, I.M., Korsch, R.J., Kennett, B.L.N., Cutten, H.N., Goodwin, J., Blay, O., Blewett, R.S., Joly, A., 2013. Crustal architecture of the Capricorn Orogen, Western Australia and associated metallogeny. Aust. J. Earth Sci. 60, 681–705.
Kaislaniemi, L., van Hunen, J., 2014. Dynamics of lithospheric thinning and mantle melting by edge-driven convection: Application to Moroccan Atlas mountains. Geochem. Geophys. Geosyst. 15, 3175–3189.
Kennett, B.L., Fichtner, A., Fishwick, S., Yoshizawa, K., 2013. Australian seismological reference model (AuSREM): mantle component. Geophys. J. Int. 192, 871–887.
Khan, A., Zunino, A., Deschamps, F., 2013. Upper mantle compositional variations and discontinuity topography imaged beneath Australia from Bayesian inversion of surface-wave phase velocities and thermochemical modeling. J. Geophys. Res. Solid Earth 118, 5285–5306.
Kirkland, C.L., Spaggiari, C.V., Pawley, M.J., Wingate, M.T.D., Smithies, R.H., Howard, H.M., Tyler, I.M., Belousova, E.A., Poujol, M., 2011. On the edge: U-Pb, Lu–Hf, and Sm–Nd data suggests reworking of the Yilgarn craton margin during formation of the Albany-Fraser Orogen. Precambr. Res. 187, 223–247.
Koptev, A., Calais, E., Burov, E., Leroy, S., Gerya, T., 2015. Dual continental rift systems generated by plume–lithosphere interaction. Nat. Geosci. 8, 388–392.
Korsch, R.J., Blewett, R.S., Smithies, R.H., Quentin de Gromard, R., Howard, H.M., Pawley, M.J., Carr, L.K., Hocking, R.M., Neumann, N.L., Kennett, B.L.N., 2013. Geodynamic implications of the Yilgarn Craton–Officer Basin–Musgrave Province (YOM) deep seismic reflection survey: part of a∼ 1800 km transect across Western Australia from the Pinjarra Orogen to the Musgrave Province, Yilgarn craton–Officer Basin–Musgrave Province (YOM) Seismic and MT workshop, pp. 169-197.
Korsch, R.J., Doublier, M.P., 2016. Major crustal boundaries of Australia, and their significance in mineral systems targeting. Ore Geol. Rev. 76, 211–228.
Lindsay, M.D., Occhipinti, S., Laflamme, C., Aitken, A., Ramos, L., 2020. Mapping undercover: Integrated geoscientific interpretation and 3D modelling of a Proterozoic basin. Solid Earth 11, 1053–1077.
Markwitz, V., Kirkland, C.L., Evans, N.J., 2017. Early Cambrian metamorphic zircon in the northern Pinjarra Orogen: Implications for the structure of the West Australian Craton margin. Lithosphere 9, 3–13.
Mazzucchelli, M., Rivalenti, G., Brunelli, D., Zanetti, A., Boari, E., 2008. Formation of Highly Refractory Dunite by Focused Percolation of Pyroxenite-Derived Melt in the Balmuccia Peridotite Massif (Italy). J. Petrol. 50, 1205–1233.
McNutt, M.K., 1998. Superswells. Rev. Geophys. 36, 211–244.
Menzies, M., Xu, Y., Zhang, H., Fan, W., 2007. Integration of geology, geophysics and geochemistry: A key to understanding the North China Craton. Lithos 96, 1–21.
Mitchell, R.N., Zhang, N., Salminen, J., Liu, Y., Spencer, C.J., Steinberger, B., Murphy, J. B., Li, Z.-X., 2021. The supercontinent cycle. Nature Rev. Earth Environ. 2, 358–374.
Mole, D.R., Kirkland, C.L., Fiorentini, M.L., Barnes, S.J., Cassidy, K.F., Isaac, C., Belousova, E.A., Hartnady, M., Thebaud, N., 2019. Time-space evolution of an Archean craton: A Hf-isotope window into continent formation. Earth Sci. Rev. 196, 102831.
Mulder, J.A., Cawood, P.A., 2021. Evaluating preservation bias in the continental growth record against the monazite archive. Geology 50, 243–247.
Nelson, D., 1999. 153903: basalt, Empress 1A, Geochronology Record 254, p. 2.
Occhipinti, S., Hocking, R., Lindsay, M., Aitken, A., Copp, I., Jones, J., Sheppard, S., Pirajno, F., Metelka, V., 2017. Paleoproterozoic basin development on the northern Yilgarn Craton, Western Australia. Precambr. Res. 300, 121–140.
Occhipinti, S.A., Tyler, I.M., Spaggiari, C.V., Korsch, R.J., Kirkland, C.L., Smithies, R.H., Martin, K., Wingate, M.T.D., 2018. Tropicana translated: a foreland thrust system imbricate fan setting for c. 2520 Ma orogenic gold mineralization at the northern margin of the Albany-Fraser Orogen, Western Australia. Geol. Soc. Lond. Spec. Publ. 453, 225–245.
Piechocka, A.M., Sheppard, S., Fitzsimons, I.C.W., Johnson, S.P., Rasmussen, B., Jourdan, F., 2018. Neoproterozoic 40Ar/39Ar mica ages mark the termination of a billion years of intraplate reworking in the Capricorn Orogen, Western Australia. Precambr. Res. 310, 391–406.
Qashqai, M.T., Afonso, J.C., Yang, Y., 2016. Multi-observable probabilistic inversion for the thermochemical structure of the lithosphere. Department of Earth and Planetary Sciences, Macquarie University.
Quentin de Gromard, R., Kirkland, C.L., Howard, H.M., Wingate, M.T.D., Jourdan, F., McInnes, B.I.A., Daniščík, M., Evans, N.J., McDonald, B.J., Smithies, R.H., 2019. When will it end? Long-lived intracontinental reactivation in central Australia. Geosci. Front. 10, 149–164.
Ramos, L.N., Aitken, A.R.A., Occhipinti, S.M., Lindsay, M.D., 2021. Rift Structures and Magmatism focus VMS and Gold mineralisation in the Paleoproterozoic Bryah Rift Basin, Australia. Ore Geol. Rev. 104192.
Rasmussen, B., Fletcher, I.R., 2002. Indirect dating of mafic intrusions by SHRIMP U-Pb analysis of monazite in contact metamorphosed shale: an example from the Palaeoproterozoic Capricorn Orogen, Western Australia. Earth Planet. Sci. Lett. 197, 287–299.
Rasmussen, B., Fletcher, I.R., Bekker, A., Muhling, J.R., Gregory, C.J., Thorne, A.M., 2012. Deposition of 1.88-billion-year-old iron formations as a consequence of rapid crustal growth. Nature 484, 498–501.
Rasmussen, B., Fletcher, I.R., Bengtson, S., McNaughton, N.J., 2004. SHRIMP U-Pb dating of diagenetic xenotime in the Stirling Range Formation, Western Australia: 1.8 Billion year minimum age for the Stirling biota. Precambr. Res. 133, 329–337.
Scibiorski, E., Tohver, E., Jourdan, F., Kirkland, C.L., Spaggiari, C., 2016. Cooling and exhumation along the curved Albany-Fraser orogen, Western Australia. Lithosphere 8, 551–563.
Smithies, R.H., Howard, H.M., Evins, P.M., Kirkland, C.L., Kelsey, D.E., Hand, M., Wingate, M.T.D., Collins, A.S., Belousova, E., 2011. High-Temperature Granite Magmatism, Crust-Mantle Interaction and the Mesoproterozoic Intracontinental Evolution of the Musgrave Province, Central Australia. J. Petrol. 52, 931–958.
Smithies, R.H., Kirkland, C.L., Korhonen, F.J., Aitken, A.R.A., Howard, H.M., Maier, W. D., Wingate, M.T.D., Quentin de Gromard, R., Gessner, K., 2015. The Mesoproterozoic thermal evolution of the Musgrave Province in central Australia — Plume vs. the geological record. Gondw. Res. 27, 1419–1429.
Spaggiari, C.V., Kirkland, C.L., Smithies, R.H., Wingate, M.T.D., Belousova, E.A., 2015. Transformation of an Archean craton margin during Proterozoic basin formation and magmatism: The Albany-Fraser Orogen, Western Australia. Precambr. Res. 266, 440–466.
Stark, J.C., Wang, X.-C., Denyszyn, S.W., Li, Z.-X., Rasmussen, B., Zi, J.-W., Sheppard, S., Liu, Y., 2019. Newly identified 1.89 Ga mafic dyke swarm in the Archean Yilgarn Craton, Western Australia suggests a connection with India. Precambr. Res. 329, 156–169.
Tang, Y.J., Zhang, H.F., Ying, J.F., Su, B.X., 2013. Widespread refertilization of cratonic and circum-cratonic lithospheric mantle. Earth Sci. Rev. 118, 45–68.
Tappe, S., Foley, S.F., Stracke, A., Romer, R.L., Kjarsgaard, B.A., Heaman, L.M., Joyce, N., 2007. Craton reactivation on the Labrador Sea margins: 40Ar/39Ar age and Sr–Nd–Hf–Pb isotope constraints from alkaline and carbonatite intrusives. Earth Planet. Sci. Lett. 256, 433–454.
Tesauro, M., Kaban, M.K., Aitken, A.R.A., 2020. Thermal and Compositional Anomalies of the Australian Upper Mantle From Seismic and Gravity Data. Geochem. Geophys. Geosyst. 21. e2020GC009305.
Tesauro, M., Kaban, M.K., Mooney, W.D., Cloetingh, S.A.P.L., 2014. Density, temperature, and composition of the North American lithosphere - New insights from a joint analysis of seismic, gravity, and mineral physics data: 2. Thermal and compositional model of the upper mantle. Geochem. Geophys. Geosyst. 15, 4808–4830.
Thebaud, N., Zwingmann, H., 2012. Dating brittle deformation in the Archean Yilgarn Craton, Western Australia, AGU Fall Meeting Abstracts.
Vallini, D.A., Rasmussen, B., KrapeŽ, B., Fletcher, I.R., McNaughton, N.J., 2005. Microtextures, geochemistry and geochronology of authigenic xenotime: constraining the cementation history of a Palaeoproterozoic metasedimentary sequence. Sedimentology 52, 101–122.
Walter, M.R., Veevers, J.J., Calver, C.R., Grey, K., 1995. Neoproterozoic stratigraphy of the Centralian Superbasin, Australia. Precambr. Res. 73, 173–195.
Wang, X.-C., Li, Z.-X., Li, J., Pisarevsky, S.A., Wingate, M.T.D., 2014. Genesis of the 1.21 Ga Marnda Moorn large igneous province by plume–lithosphere interaction. Precambr. Res. 241, 85–103.
Wang, Z., Kusky, T.M., Capitanio, F.A., 2018. On the Role of Lower Crust and Midlithosphere Discontinuity for Cratonic Lithosphere Delamination and Recycling. Geophys. Res. Lett. 45, 7425–7433.

Weber, U.D., Kohn, B.P., Gleadow, A.J.W., Nelson, D.R., 2005. Low temperature Phanerozoic history of the Northern Yilgarn Craton, Western Australia. Tectonophysics 400, 127–151.
Wenker, S., Beaumont, C., 2018. Can metasomatic weakening result in the rifting of cratons? Tectonophysics 746, 3–21.
Wingate, M., 2007. Proterozoic mafic dykes in the Yilgarn Craton. Geoscience Australia Record 2007, 80–83.
Wingate, M., Bodorkos, S., Kirkland, C.L., 2008. 178113: gabbro sill, Kurrajong Bore. Geochronology Record 732, 7.
Wingate, M.T.D., Pirajno, F., Morris, P.A., 2004. Warakurna large igneous province: A new Mesoproterozoic large igneous province in west-central Australia. Geology 32, 105–108.
Xu, Y.G., 2001. Thermo-tectonic destruction of the archaean lithospheric keel beneath the Sino-Korean Craton in China: Evidence, timing and mechanism. Phys. Chem. Earth Part A. 26, 747–757.
Yoshida, M., 2010. Temporal evolution of the stress state in a supercontinent during mantle reorganization. Geophys. J. Int. 180, 1–22.
Yoshida, M., Santosh, M., 2011. Supercontinents, mantle dynamics and plate tectonics: A perspective based on conceptual vs. numerical models. Earth Sci. Rev. 105, 1–24.
Yoshizawa, K., 2014. Radially anisotropic 3-D shear wave structure of the Australian lithosphere and asthenosphere from multi-mode surface waves. Phys. Earth Planet. In. 235, 33–48.
Yoshizawa, K., Kennett, B.L.N., 2015. The lithosphere-asthenosphere transition and radial anisotropy beneath the Australian continent. Geophys. Res. Lett. 42, 3839–3846.
Yuan, H., 2015. Secular change in Archaean crust formation recorded in Western Australia. Nat. Geosci. 8, 808–813.
Zhang, N., Dang, Z., Huang, C., Li, Z.-X., 2018. The dominant driving force for supercontinent breakup: Plume push or subduction retreat? Geosci. Front. 9, 997–1007.
Zheng, J.P., Griffin, W.L., Ma, Q., O'Reilly, S.Y., Xiong, Q., Tang, H.Y., Zhao, J.H., Yu, C. M., Su, Y.P., 2012. Accretion and reworking beneath the North China Craton. Lithos 149, 61–78.
Zhong, S., Zhang, N., Li, Z.-X., Roberts, J.H., 2007. Supercontinent cycles, true polar wander, and very long-wavelength mantle convection. Earth Planet. Sci. Lett. 261, 551–564.